

Fabrication of mesoscopic superconducting Nb wires using conventional electron-beam lithographic techniques

Nam Kim, Klavs Hansen, Jussi Toppari, Tarmo Suppula, and Jukka Pekola
Department of Physics, University of Jyväskylä, P.O. Box 35, FIN-40351 Jyväskylä, Finland

(Received 11 July 2001; accepted 26 November 2001)

Conventional electron-beam lithography has been used to fabricate mesoscopic Nb wires. Nb was deposited in an ultrahigh vacuum evaporation chamber using electron gun heating. The typical linewidth and the thickness were 200 and 50 nm, respectively. The transition temperatures were above 7 K. They increased with thickness and linewidth. To demonstrate the feasibility of two angle evaporation techniques, we also fabricated Nb/(Al-)AlO_x/Nb tunnel junctions showing superconducting single-electron transistor characteristics. © 2002 American Vacuum Society. [DOI: 10.1116/1.1445168]

A number of nanometer-scale devices such as single-electron transistors (SETs),¹ superconducting quantum bits,² and other mesoscopic superconducting devices³ have been realized using the self-alignment technique which provides submicron accuracy.⁴ Self-alignment is achieved by shadow evaporation, commonly used with the polymethylmethacrylate (PMMA) and co-polymer [P(MMA-MAA)] resists as a double layer stencil mask patterned by electron-beam (e-beam) lithography. Until now this conventional shadow evaporation technique has been applied successfully for soft metals like Al, Cu, and Pb. For the refractory metals such as Nb, W, or Ta, however, it is known to be difficult to apply.^{5,6} In particular, Nb is a promising alternative to the soft metals for superconducting nano devices because of its large superconducting gap and high stability under thermal cycling.

Two different methods have been tried to make Nb-based submicron devices. One is the self-alignment technique with a stencil mask consisting of resist polymers. The authors of Ref. 5 used a four-layer mask composed of PMMA resist layers and one Ge layer. The Ge layer was expected to withstand the mechanical strain due to the Nb layer during its evaporation. The Nb film made this way was not of good quality because its transition temperature T_c was far below that of bulk Nb. This degradation of the Nb film was believed to be due to the contamination of the Nb layer by outgassing from the resists during the Nb evaporation. To circumvent this problem the authors of Ref. 6 used as a mask Phenylene-ether-sulfone (PES) polymer, which has a glass temperature and a decomposition temperature much higher than those of PMMA resist. With this new process a Nb wire of 0.15 μm width and 60 nm thickness showed a T_c of 7.1 K. However, this PES process requires more steps in the fabrication than the conventional PMMA double layer process. The second method is the multilayer technique by which Nb/(Al-)AlO_x/Nb trilayers are formed *in situ*, followed by the fabrication process *ex situ*.⁷⁻⁹ In spite of the reliability of the insulating layer and the high-quality superconducting Nb electrodes, the complicated multilayer process makes it more difficult to reduce the size of junctions and align the electrodes on the submicron scale than the self-alignment techniques. Thus it would be highly welcomed to demonstrate

that high-quality submicron Nb structures can be fabricated by conventional e-beam lithography.

Problems with applying the conventional technique have been ascribed to the partial decomposition of the PMMA co-polymer double layer during the evaporation of the refractory metals.^{5,6} The resulting outgassing from the resist^{5,6} and consequent contamination of the deposited Nb would then explain the changes in the electronic properties of the deposited Nb. The other question raised by the authors of Ref. 5 is that the PMMA resist layer is not strong enough to withstand the strain during the evaporation of the Nb film. Contrary to this common experience, we show here that it is possible to fabricate mesoscopic Nb wires with zero-field critical temperatures T_c higher than 7.0 K by using the conventional shadow evaporation technique.

Our results were obtained with a standard e-beam lithography process that followed the most common procedures and conventional recipes. We deposited a double layer of PMMA-P(MMA-MAA) on oxidized Si substrate. The SiO₂ layer was about 250 nm thick. The spinning rates for PMMA and P(MMA-MAA) were 3000 and 6000 rpm, respectively, and the spinning time was 30 s for both. The thickness of the PMMA and P(MMA-MAA) were measured to be about 270 and 300 nm, respectively. The resist was baked at 160 °C for about 60 min. We then drew the pattern (see Fig. 1) using a scanning electron microscope (JEOL, JSM 840A). The linewidth was about 200 nm for this sample. To develop the upper layer of the PMMA resist we immersed the sample in a mixed (1:2) solution of methyl *iso*-butyl ketone and isopropyl alcohol for 12 s. To develop the lower layer of the P(MAA-MAA) resist and to form an undercut, the sample was dipped into a solution (1:2) of methyl glycol and methanol for 15 s. Nb (99.9%, Goodfellow) was then evaporated onto the patterned substrate in an ultrahigh vacuum (UHV) chamber equipped with a cryo-vacuum pump (Cryo-Torr high vacuum pump, CTI-Cryogenics) and a liquid-nitrogen trap. The pressure inside the UHV chamber was 2×10^{-8} mbar, the evaporation rate was about 0.45 nm/s, and the power of the electron gun was 2 kW.

Table I summarizes the properties of the investigated samples. The wires are typically about 200 nm wide and 11

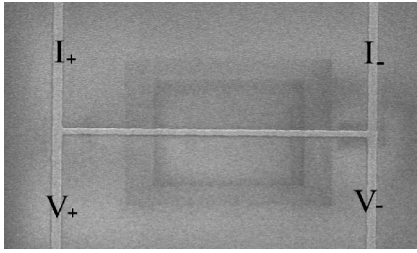


Fig. 1. Scanning electron micrograph of a Nb wire with thickness 45 nm and width 200 nm. The wire is 11 μm long.

μm long, while the width of the two-dimensional (2D) film is about 10 μm . We have measured the resistance R as a function of temperature T in the standard four probe measurement configuration with a lock-in amplifier (see Fig. 1). The constant excitation currents were 10 nA for wires and 100 nA for 2D films. The temperature was monitored by a calibrated diode sensor (DT470, Lake Shore Cryotronics). Figure 2 shows five representative $R(T)$ curves.

All samples became superconducting, but the transition temperature T_c depended on the sample dimension. T_c was defined as the temperature where the sample resistance is reduced to one-half of its value at 10 K. One of the samples, the 2D Nb film with a thickness of 150 nm (2D-1) showed $T_c = 9.1$ K, close to $T_c = 9.26$ K of bulk Nb (see the inset of Fig. 2). We have found that the superconducting transition temperature decreases with Nb thickness or width as shown in Fig. 2 and Table I. Wire-3 with dimensions typically used in applications had a T_c of 7.0 K, $\rho_{10\text{K}}$ of 33 $\mu\Omega\text{cm}$, and the resistivity ratio (RRR) $\rho_{295\text{K}}/\rho_{10\text{K}}$ of 1.5. These characteristic values are very close to those¹⁰ reported in Ref. 6. The transition width ΔT of our wires ranged from 62 to 232 mK, comparable to $\Delta T \approx 200$ mK shown by thin Nb films without any contamination due to resist.¹¹ Thus, the electrical characteristics ρ , T_c , and ΔT shown by our wire samples indicated that contamination due to the PMMA resist could be as low as that of the PES resist. In addition, we want to stress that we have not observed any deformation of PMMA double layers after Nb evaporation contrary to Ref. 5. We believe that a crucial feature for the success of our experiments in the evaporation chamber was the 40 cm distance between the

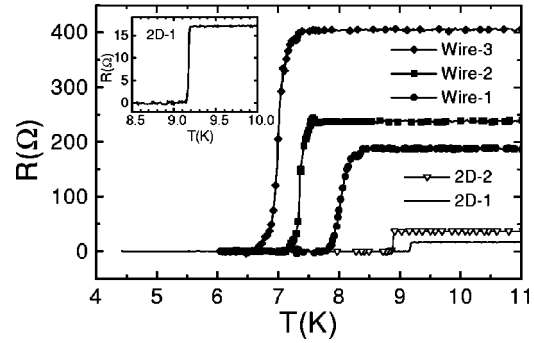


Fig. 2. Resistance vs temperature for the various samples. Inset: resistance vs temperature for sample 2D-1 on an expanded scale.

substrate and the Nb crucible. This relatively large separation reduced the heating of the samples when evaporating Nb.

Figure 3 shows transition temperature T_c vs sheet resistance R_{sheet} where R_{sheet} increases as the sample thickness or width decreases. T_c decreases at a rate $dT_c/dR_{\text{sheet}} \approx -311$ mK/ Ω which is an order of magnitude higher than reported by other groups^{11–13} based on Nb films deposited without any resist stencil mask. To understand the dependence of T_c on R_{sheet} we need to cover a wider range of sheet resistance data. The inset of Fig. 3 shows how the resistivity at 10 K depends on the sheet resistance. Contrary to amorphous MoGe films, which showed an order of magnitude higher resistivity ($\rho \approx 160\text{--}200$ $\mu\Omega\text{cm}$),¹⁴ Nb films have a strong $\rho(R_{\text{sheet}})$ dependence, independent of how they have been fabricated.^{11–13} There is no satisfactory explanation for this strong $\rho(R_{\text{sheet}})$ dependence of Nb films yet.

To also demonstrate the feasibility of the conventional two angle evaporation technique and to take advantage of the high critical temperatures reached, we have also fabricated Nb/(Al–)AlO_x/Nb junctions with a single-electron transistor geometry (the inset of Fig. 4). The 20-nm-thick Al layer was evaporated on the 53-nm-thick Nb layer. The Al layer was subsequently oxidized in a static oxygen pressure of 100 mbar for 5 min. Then the third layer of Nb was deposited at a different angle. We measured the current vs voltage (I – V) characteristic at temperatures below 200 mK for the Nb/(Al–)AlO_x/Nb junctions with a total normal resistance

TABLE I. Results of the various samples. We denote as 2D films the macroscopic samples with width 10 μm . w , t , L , ρ , and R_{sheet} are the sample width, thickness, length, resistivity, and sheet resistance at 10 K. $\rho_{295\text{K}}/\rho_{10\text{K}}$ is the resistivity ratio (RRR) for the two temperatures, 295 and 10 K. The transition width ΔT is defined as the temperature range where the resistance falls between 20%–80% of the normal resistance at 10 K.

Sample	w (μm)	t (nm)	L (μm)	T_c (K)	ρ ($\mu\Omega\text{cm}$)	R_{sheet} (Ω)	$\rho_{295\text{K}}/\rho_{10\text{K}}$	ΔT (mK)
2D-1	10	150	300	9.1	7.6	0.56		14
2D-2	10	67	160	8.9	15	2.2	2.2	13
2D-3	10	53	145	8.4	15	2.8	2.1	11
2D-4	10	53	160	8.3	16	3.0	2.0	9
2D-5	10	45	160	8.3	7.4	1.7		97
Wire-1	0.23	67	11	8.0	27	4.0		190
Wire-2	0.23	45	11	7.3	23	5.1	1.6	100
Wire-3	0.20	45	11	7.0	33	7.3	1.5	150
Wire-4	0.30	67	11	8.1	19	2.8	1.9	62
Wire-5	0.25	53	11	7.3	31	5.8	1.6	232

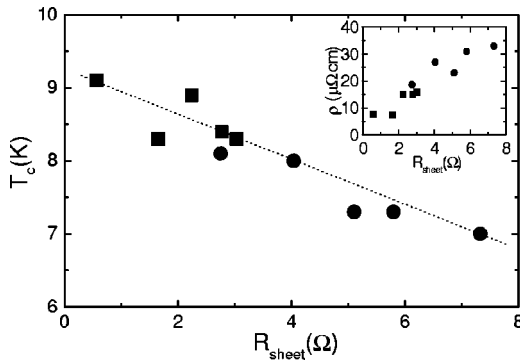


FIG. 3. T_c vs R_{sheet} . 2D samples (solid square) and wire samples (solid circle). The dotted line has a slope of $dT_c/dR_{\text{sheet}} = -311$ mK/Ω. Inset shows ρ vs R_{sheet} at 10 K.

R_n of 75 kΩ (Fig. 4). The I - V curve clearly shows a superconducting gap, $\Delta_{\text{Nb}} \approx 0.75$ meV (see the inset of Fig. 4). This is about 66% of the expected value, assuming T_c of both electrodes and island is 7 K. The suppression of the superconducting gap could be due to the existence of an Al layer. The total film thickness of Nb and a not-fully oxidized Al could be considered 106 nm and at most 20 nm, respectively. If we apply the proximity model in the Cooper limit¹⁵ for a rough estimate, assuming the dimensionless electron-phonon coupling constant $\lambda = 0.82$,¹⁶ the Nb gap could be suppressed to 79% of the one without proximity effect.¹⁷ This agrees reasonably well with our experiments.

We also measured gate modulated current as a function of bias voltage V_b (Fig. 5). From the period of the gate modulation we estimate the gate capacitance C_g to be 15 aF, which coincides with that of Al/AIO_x/Al SET fabricated by us with the same geometry. The Josephson coupling energy $E_J = (h/4e^2) \cdot (\Delta_{\text{Nb}}/2R_n) \approx 32$ μeV is comparable to the charging energy $E_c \approx 35$ μeV which was determined from the I - V curves as function of gate voltages (not shown here). Thus in order to have charging energy dominant over the Josephson

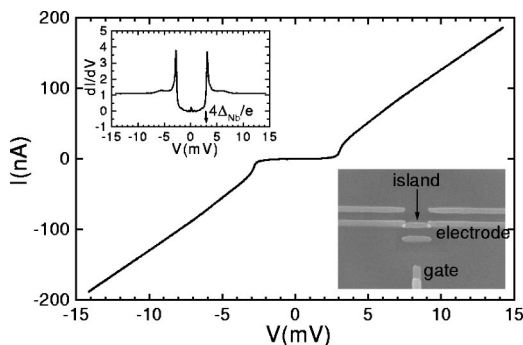


FIG. 4. I - V characteristic of the Nb/(Al-AIO_x)/Nb SET at a temperature below 200 mK. Inset (upper left): the dynamic conductance dI/dV vs voltages V . $\Delta_{\text{Nb}} = 0.75$ meV. Inset (lower right): scanning electron micrograph of the Nb/(Al-AIO_x)/Nb junctions fabricated by conventional two angle evaporation. The width of Nb wire (electrode) is about 0.24 μm.

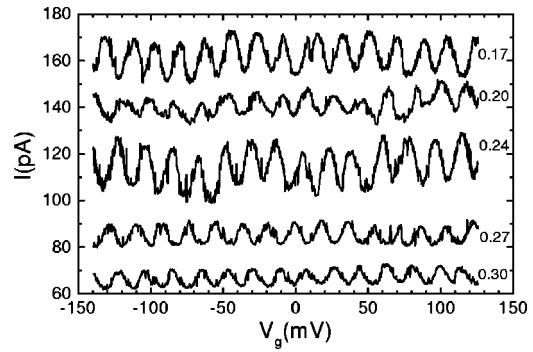


FIG. 5. Current I through the junctions vs gate voltage V_g as a function of bias voltage V_b at a temperature below 200 mK. V_b is displayed in units of mV on the right-hand side of each curve. Each curve is displaced in y axis for clarity.

coupling energy, we either have to increase the junction resistance or decrease the junction area.

In conclusion, we have demonstrated that the conventional e-beam lithographic technique can be used to fabricate mesoscopic 200-nm-wide Nb wires with T_c above 7.0 K. We have successfully applied this technique to the fabrication of Nb/(Al-AIO_x)/Nb SET whose superconducting gap is about 66% of the expected value.

This work has been supported by the Academy of Finland under the Finnish Center of Excellence Program 2000-2005 (Project No. 44875, Nuclear and Condensed Matter Program at JYFL) and the EU (Contract IST-1999-10673). The authors thank K. Gloos and J. Kim for discussions.

¹Single Charge Tunneling, edited by H. Grabert and M. H. Devoret (Plenum, New York, 1992).

²Y. Nakamura, Yu. A. Pashkin, and J. S. Tsai, Nature (London) **398**, 786 (1999).

³Proceedings of the NATO Advanced Research Workshop, Mesoscopic Superconductivity, edited by F. W. Hekking, G. Schön, and D. V. Averin, Physica B **203** (1994).

⁴G. J. Dolan and J. H. Dunsmuir, Physica B **152**, 7 (1988).

⁵Y. Harada, D. B. Haviland, P. Delsing, C. D. Chen, and T. Claeson, Appl. Phys. Lett. **65**, 636 (1994).

⁶P. Dubos, P. Charlat, Th. Crozes, P. Paniez, and B. Pannetier, J. Vac. Sci. Technol. B **18**, 122 (2000).

⁷A. B. Pavolotsky, Th. Weimann, H. Scherer, V. A. Krupenin, J. Niemeyer, and A. B. Zorin, J. Vac. Sci. Technol. B **17**, 230 (1999).

⁸V. Patel and J. E. Lukens, IEEE Trans. Appl. Supercond. **9**, 3247 (1999).

⁹K. Blüthner, M. Götz, W. Krech, H. Mühlig, Th. Wagner, H.-J. Fuchs, D. Schelle, L. Fritzsche, B. Nachtmann, and A. Nowack, J. Phys. IV **6**, C3-163 (1996).

¹⁰In Ref. 6 Nb wires with 0.15 μm width and 60 nm thickness showed T_c of 7.1 K and RRR of 1.6. The resistivity was in the range of 17–20 μΩ cm for Nb wires with 0.3 μm width.

¹¹B. J. Dalrymple, S. A. Wolf, A. C. Ehrlich, and D. J. Gillespie, Phys. Rev. B **33**, 7514 (1986).

¹²M. Hikita, Y. Tajima, and T. Tamamura, Phys. Rev. B **42**, 118 (1990).

¹³J. H. Quateman, Phys. Rev. B **34**, 1948 (1986).

¹⁴J. M. Graybeal and M. R. Beasley, Phys. Rev. B **29**, 4167 (1984); A. Bezryadin, C. N. Lau, and M. Tinkham, Nature (London) **404**, 971 (2000).

¹⁵N. R. Werthamer, Phys. Rev. **132**, 2440 (1963); G. Deutscher and P. G. de Gennes, in Superconductivity, edited by R. D. Parks (Marcel Dekker, New York, 1969).

¹⁶C. P. Poole, Jr., H. A. Farach, and R. J. Creswick, Superconductivity (Academic, New York, 1995), p. 60.

¹⁷We assumed the dimensionless electron-phonon coupling constant λ to be 0.82 in the BCS formula $\Delta = 2\hbar\omega_D \exp(-1/\lambda)$.